Letter

Dirac polaron dynamics in the correlated semimetal of perovskite $CaIrO_3$

J. Fujioka,[1] R. Yamada,[2] T. Okawa,[2] and Y. Tokura[2,3,4]

[1]*Faculty of Material Science, University of Tsukuba, 1-1-1 Tennodai, Tsukuba, Ibaraki 305-8573, Japan*

[2]*Department of Applied Physics, University of Tokyo, Hongo, Tokyo 113-8656, Japan*

[3]*RIKEN Center for Emergent Matter Science (CEMS), Wako 351-0198, Japan*

[4]*Tokyo College, University of Tokyo, Hongo, Tokyo 113-8656, Japan*

(Received 22 July 2020; accepted 7 January 2021; published 19 January 2021)

We have investigated the charge dynamics of the correlated Dirac semimetallic perovskite $CaIrO_3$ by infrared spectroscopy. The optical conductivity spectra show the ω-linear-type interband transition and a tiny Drude response at low temperatures, suggesting that the Dirac node is pinned near the Fermi energy due to the Mott criticality. Moreover, a large polaron absorption appears at around 0.04 eV, when thermally excited carriers diminish and the plasma frequency decreases below the optical phonon energy. The electron correlation and resultant reduced plasma frequency are likely to enhance the electron-phonon interaction via the insufficient electronic screening, realizing the Dirac polaron.

DOI: 10.1103/PhysRevB.103.L041109

The quantum phenomena in topological (Dirac/Weyl) semimetals are subjects of great interest in the condensed matter science. One of the remarkable features of topological semimetal is that highly mobile Dirac/Weyl electrons give rise to unconventional quantum phenomena as exemplified by the giant-magnetoresistance and anomalous/spin Hall effect [1]. Thus far, many studies have focused on the phenomena described by the single-particle physics, but there is a growing interest in the effect of strong electron correlation as a unique pathway to explore emergent quantum phenomena. In general, the electron correlation not only renormalizes an effective mass or Fermi velocity of electron, but also promotes several electronic interactions including the magnetic exchange interaction and electron-phonon interaction, which are important to realize unconventional topological phases. In particular, recent studies argue that the axionic charge density wave or excitonic insulator can be induced, given that the electron correlation or electron-phonon interaction is sufficiently strong [2–6].

In this context, the topological semimetal coupled to the Mott criticality may offer a fertile ground to study unconventional topological phases of correlated Dirac/Weyl electrons [7–10]. The perovskite $AIrO_3$ (A=Ca, Sr, Ba) [see Fig. 1(a)] is a candidate of the Dirac semimetal near the Mott transition, which is characterized by the strong electron correlation and relativistic spin-orbital coupling due to the Ir 5d electron [11–13]. In particular, the electronic state nearby the Fermi level (E_F) is dominated by a nearly half-filled Ir 5d state with $J_{eff} = 1/2$ pseudospin [10,14], resulting in the compensated semimetal with electron pockets with the Dirac nodal line near the U point and a massive hole pocket near the Γ point [see Figs. 1(b)–1(d)]. In a series of $AIrO_3$, the effective one-electron bandwidth can be varied by tuning the Ir-O-Ir bond angle (ϕ) depending on the ionic radius of the A-site ion [Fig. 1(a)] [15]; the largest $GdFeO_3$-type lattice distortion results in the largest effective electron correlation in the $CaIrO_3$.

The recent experiments have uncovered that the line node is nearly pinned to E_F (about 10 meV below E_F) due to the Mott criticality, leading to the Dirac electrons with the dilute carrier density about 2×10^{17} cm^{-3} and mobility exceeding 60 000 cm^2/Vs at low temperatures [16–18]. In particular, when the system reaches the quantum limit, wherein the electrons are quasi-one-dimensionally confined by the magnetic field, the resistivity steeply increases, yielding the longitudinal magnetoresistance with a ratio of 5500%. On the contrary, a more conventional metallic state with higher carrier density is realized in $SrIrO_3$ and $BaIrO_3$ [13] with the smaller $GdFeO_3$-type lattice distortion and effective electron correlation. The effective electron correlation and/or electron-phonon interaction likely play crucial roles for the transport of Dirac electron in these materials, yet the electronic interaction has been poorly understood. In this study, we have investigated the charge dynamics of $CaIrO_3$ by means of optical spectroscopy and found that the Dirac electron exhibits the polaronic excitation around 0.04 eV at low temperatures. It is likely that the electron correlation significantly reduces the electronic screening via the renormalized plasma frequency, promoting the Frohlich (long-range) electron-phonon interaction and formation of highly mobile polaronic Dirac electrons (Dirac polarons).

The samples of $CaIrO_3$ were grown at 1300 °C under 1 GPa by using the cubic anvil-type high-pressure facility. The obtained crystal is the densely packed assembly of the single crystalline grain with typical size of about 0.2–0.4 mm. We polished the exposed surface of unoriented grain and measured the reflectivity spectra with unpolarized light [19]. Since the Fermi surface and crystal structure are not significantly anisotropic [16], it is reasonable to consider that the intra/interband optical transition does not show

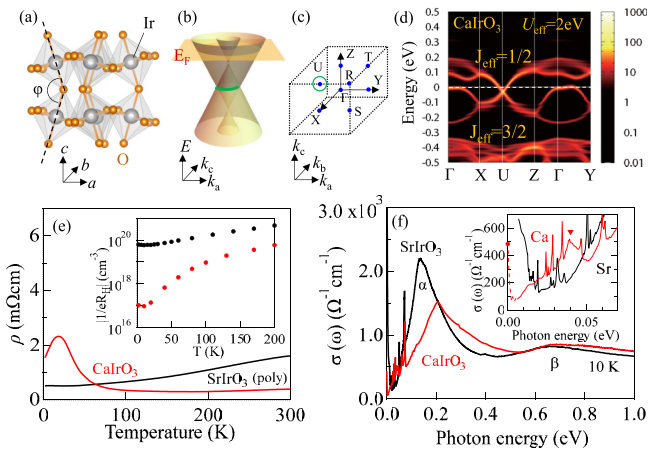

FIG. 1. (a) The crystal structure of $CaIrO_3$. Illustration of (b) Dirac band dispersion and (c) location of line node (green line) in the momentum space. The line node is on the $k_b{=}\pi$ plane. (d) The band structure derived by the theoretical calculation employing the dynamical mean field theory (Ref. [16]). The color code (dashed line) represents the spectral intensity (E_F). (e) Resistivity for single crystalline $CaIrO_3$ and polycrystalline $SrIrO_3$. The inset shows the inverse of the Hall coefficient. (f) $\sigma(\omega)$ spectra at 10 K. Inset shows the magnified view of the low energy region. The triangle indicates peak A. The circle and dashed line denote the dc conductivity and the expected spectra from the Hagen-Rubens extrapolation, respectively.

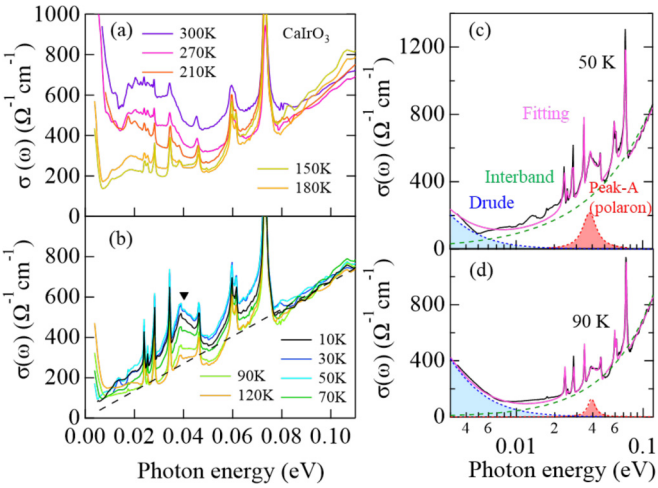

FIG. 2. The optical conductivity spectra (a) above 150 K and (b) below 120 K. The triangle indicates peak A. The dashed line denotes the fitting results for interband transition at 10 K (see also the text). The fitting results (c) at 50 K and (d) at 90 K, respectively (magenta lines). The Drude response, interband transition, and peak A (polaron band) are shown by blue, green, and red dotted lines.

remarkable polarization or crystal-orientation dependence in the low-energy region. The spectra in the region 0.02–0.7 eV (0.5–5 eV) are measured by using a Fourier transform (grating) type spectrometer equipped with microscope, while those in the region 0.004–0.1 eV are also measured for a lump of grains with using macro-optics. The results obtained by using the microscope are similar to those obtained by using macro-optics, indicating that the effect from the grain boundary is not remarkable [19]. The spectra in the region 3–40 eV are measured at room temperature in the UV-SOR. We derived the optical conductivity ($\sigma(\omega)$) spectra by the Kramers-Kronig analysis with appropriate extrapolations [19] (see Fig. S3).

The resistivity of single crystalline $CaIrO_3$ [see Fig. 1(e)] exhibits a metallic temperature dependence above 150 K, but a prominent peak is observed around 20 K [16]. As shown in the inset to Fig. 1(e), the carrier density monotonically decreases with decreasing temperature and reaches about $\sim 1 \times 10^{17}$ cm^{-3} below 20 K. We note that the resistivity peak can be explained in terms of the temperature dependence of electron density and electron mobility; the former (latter) decreases (increases) as temperature decreases, the balance of which causes the resistivity peak. This behavior is in contrast with the case of $SrIrO_3$, wherein the resistivity shows a metallic behavior in all temperature region and the carrier density is as high as 6×10^{19} cm^{-3} even at 10 K.

In both $CaIrO_3$ and $SrIrO_3$, the $\sigma(\omega)$ at 10 K [see Fig. 1(f)] shows two broad peaks (α and β band), which are assigned to the optical transition from the occupied $j_{\rm eff} = 1/2$ state to the unoccupied $j_{\rm eff} = 1/2$ state, and that from the occupied $j_{\rm eff} = 3/2$ state to the unoccupied $j_{\rm eff} = 1/2$ state, respectively [see Fig. 1(d)] [14,20]. The spectral intensity of the α band, which is defined by the effective number of electrons ($N_{\rm eff}$) below 0.5 eV [19], is smaller by about 10% in $CaIrO_3$ than in $SrIrO_3$. This is consistent with the smaller one-electron bandwidth in $CaIrO_3$ than in $SrIrO_3$, since the spectral intensity of the α band is scaled to the one-electron bandwidth of the $j_{\rm eff} = 1/2$ state [14]. On the other hand, the charge dynamics below 0.1 eV is qualitatively different between these two systems [see the inset to the Fig. 1(f)]. The tail of the Drude response is observed in $SrIrO_3$, but is likely to be located below 0.004 eV in the $CaIrO_3$ [19] (see also Fig. S3). Furthermore, the $CaIrO_3$ shows an absorption peak around 0.04 eV (peak A), the shape of which is different from other sharp peaks of optical phonons.

Figures 2(a) and 2(b) display the $\sigma(\omega)$ spectra above 150 K and those below 120 K, respectively. The $\sigma(\omega)$ spectra above 150 K show the Drude response accompanied by a very broad humplike structure around 0.03 eV due perhaps to the thermally induced incoherent charge dynamics. With decreasing temperature, both structures gradually diminish; in particular, the humplike structure is no longer discernible below 150 K. On the contrary, it is clear that peak A appears below 120 K. To quantify the temperature dependence of the Drude response and peak A, we fitted the spectra using the following formula,

$$\sigma(\omega) = \frac{\sigma_D}{1+\omega^2\tau_D^2} + \frac{S_0\gamma_0\omega_0^2\omega^2}{(\omega^2-\omega_0^2)^2+\gamma_0^2\omega^2} + A\omega^\alpha + \sum_{i=1}^{9} S_i\omega\left[1 - \frac{(q_i+(\omega-\omega_i)/\gamma_i)^2}{1+(\omega-\omega_i)^2/\gamma_i^2}\right]. \quad (1)$$

The first term represents the Drude response with the dc conductivity (σ_D) and relaxation time (τ_D), respectively. The second term represents peak A with the oscillator strength (S_0), damping constant (γ_0), and peak energy (ω_0), respectively. We modeled the interband transition as the third term with the parameters A and α. The phonons are modeled by

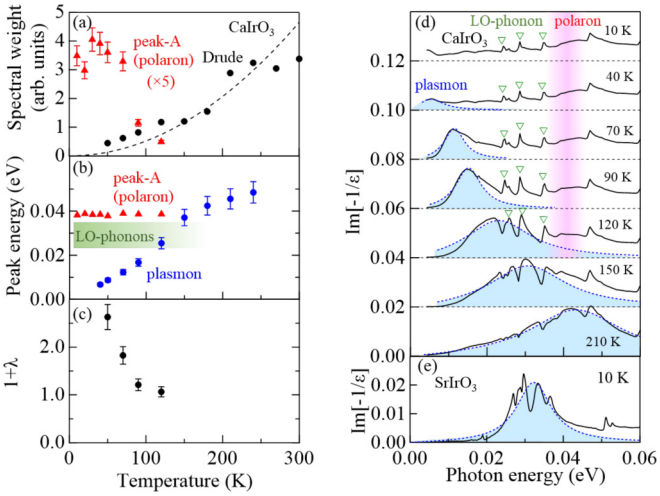

FIG. 3. (a) The spectral weight of peak A (polaron band) and Drude weight. The dashed line is the fitting result by the model (see text). (b) The temperature dependence of renormalized plasma frequency (ω_p^*) and energy of peak A (polaron band) (ω_0). The hatched region denotes the energy range of the three LO phonons [triangles in Fig. 3(d)]. (c) The mass enhancement factor $1+\lambda$. (d) The loss function spectra ($\mathrm{Im}[-1/\epsilon(\omega)]$) of $CaIrO_3$. The spectra are offset for clarity. The dotted lines (open triangles) indicate the plasmon resonance (the LO phonons). The hatched region denotes the energy range of peak A (polaron band). (e) $\mathrm{Im}[-1/\epsilon(\omega)]$ spectrum of $SrIrO_3$ at 10 K.

the fourth terms with oscillator strength (S_i), damping constant (γ_i), asymmetric parameter (q_i), and peak energy (ω_i), considering the asymmetric shape due to the electron-phonon interaction [19].

As shown in Figs. 2(c) and 2(d), the fitting nearly reproduces the experimental results. Specifically, below 70 K, the fitting yields $\alpha \sim 1$, suggesting that the interband transition spectrum is of the ω-linear type as the case of Dirac semimetals with a point node [21,22]. The theoretical study proposes that the nodal line semimetal shows the ω-linear type interband transitions, when the radius of the nodal line is sufficiently small [23]. This is consistent with the previous report that the size of the nodal line is as small as $1/60$ of the reciprocal lattice unit [16]. By assuming that the present band structure can be regarded as the nearly degenerate two Dirac cones [see Fig. 1(b)], the v_F is estimated to be $(5.6 \pm 0.1) \times 10^4$ m/s from the slope of interband transition [24].

We also calculated the spectral weight for peak A and Drude response by using the effective number of electrons N_{eff}, i.e., the energy integration of $\sigma(\omega)$ [19]. As shown in Fig. 3(a) (see also Fig. S4), the Drude weight monotonically decreases with decreasing temperature. In Dirac semimetals with finite carrier density, generally, the Drude weight is temperature independent at low temperatures, but increases as a function of temperature when the thermal excitation of carriers becomes remarkable. Specifically, at high temperatures of $k_BT > E_F$, it is predicted that the Drude weight for Dirac semimetals with a point node is described by $\pi e^2 (k_BT)^2/(18\hbar^3 v_F)$ [25,26]. By regarding the present band structure as the nearly degenerate two Dirac cones [see Figs. 1(b) and 1(d)], the experimental result agrees with the model calculation with $v_F = (5.6 \pm 0.3) \times 10^4$ m/s [see Fig. 3(a)]. This is consistent with the results of transport measurements [16], suggesting that the Drude response originates from the Dirac electrons.

On the contrary, the spectral weight of peak A rises below 120 K and appears to maximize around 30 K. To clarify the origin of peak A, we explored the plasmon resonance and longitudinal optical (LO) phonon with use of the loss function spectra $\mathrm{Im}[-1/\epsilon(\omega)]$. As shown in Fig. 3(d), at 210 K, the $\mathrm{Im}[-1/\epsilon(\omega)]$ spectra exhibit a broad peak of plasmon resonance with fine dips and peaks due to optical phonons. With decreasing temperature, the plasmon peak shifts toward lower energy and cannot be traced below 40 K. Moreover, the three LO phonons in the energy range 0.24–0.35 eV become clear below 120 K, wherein the plasma frequency is lower than their energies. In other words, the three LO phonons and the plasmon resonance form an amalgamated band at high temperatures, suggesting that the formers are strongly coupled to the latter, i.e., the Drude response. Figure 3(b) shows the energy of peak A, energy range of the three LO phonons, and the plasma frequency derived from the $\mathrm{Im}[-1/\epsilon(\omega)]$ spectra [19]. The energy of peak A is slightly higher than the energy range of the three LO phonons [see also Fig. 3(d)]. Moreover, it is likely that peak A rises when the energy of plasmon resonance decreases across the three LO phonons around 0.24–0.35 eV with decreasing temperature.

Then, we discuss the origin of peak A. Considering that the spectral intensity steeply increases below 120 K and the peak width is more than 0.01 eV, which is one order larger than those of other optical phonons [19], peak A may not be the conventional infrared active phonon. Indeed, the corresponding absorption is absent in $SrIrO_3$, which has a similar crystal structure to $CaIrO_3$ [see inset to Fig. 1(f)]. Another possibility would be the interband excitation of the Dirac band or other bands [27,28]. It is argued that the excitonic charge excitation may show a peak around the energy of $2E_F$ [29]. In the present system, however, $2E_F$ would be at most 0.02 eV [16], which may not be consistent with the observed peak energy. Although the interband transition around the Γ point appears to be possible in terms of the energy scale [see Fig. 1(d)], this is also unlikely, since the corresponding absorption is absent in $SrIrO_3$, which has a similar electronic state around the Γ point [14].

Considering the strong coupling to the LO phonons, the most plausible origin of peak A is the polaron excitation. In case of large polaron (Fröhlich polaron), the polaron excitation is usually observed as a broad absorption band emerging at higher energy side of LO phonon(s), when ω_p^* is lower than the energy of LO phonon, or equivalently, when the LO phonons are not sufficiently screened by charge carriers [30–32]. In the present case, given that the three LO phonons around 0.24–0.35 eV [Fig. 3(d)] are relevant for the polaron formation, it is reasonable that the reduction of ω_p^* induces the polaron band below 120 K [see Figs. 3(a) and 3(b)]. Following the Frohlich polaron model, the mass enhancement factor $v_F^b/v_F^*(=1+\lambda)$ is defined as the ratio of Drude weight to the summation of Drude weight and the polaron band. (Here, v_F^b and v_F^* are the bare and renormalized Fermi velocity, respectively.). As shown in Fig. 3(c), the $1+\lambda$ increases with decreasing temperature and reaches about 2.7 at 50 K, which

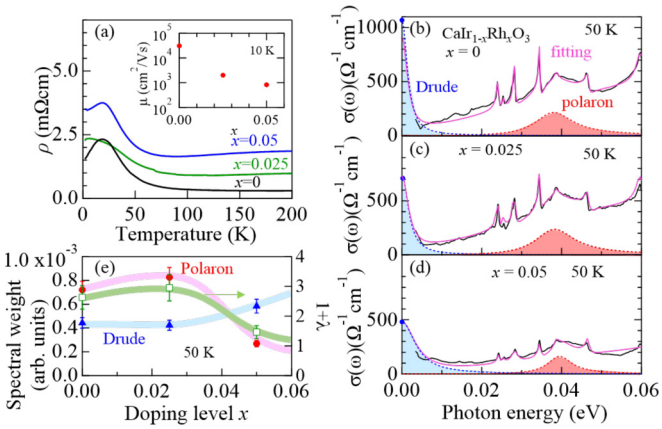

FIG. 4. (a) Temperature dependence of resistivity in $CaIr_{1-x}Rh_xO_3$. The inset shows the electron mobility at 10 K. The $\sigma(\omega)$ spectra at 50 K for (b) $x = 0$, (c) 0.025, and (d) 0.05, respectively. The magenta line denotes the fitting curve with the Drude response (blue dotted line) and polaron band (red dotted line). The closed circle at $\omega = 0$ denotes the dc conductivity. (e) The Drude weight (blue), spectral weight of polaron band (red), and the mass enhancement factor $1 + \lambda$ (green), all derived at 50 K.

corresponds to the coupling constant of Frohlich interaction $\alpha = 4.3$ [33]. We note that this scenario can naturally explain the absence of the polaron band in $SrIrO_3$; as shown in Fig. 3(e), the plasmon peak lies as high as 0.032 eV even at 10 K due to the larger carrier density and less renormalized v_F^*, which results in the reduction of the Frohlich interaction through the enhanced electronic screening. In other words, in $CaIrO_3$, it is likely that the strong electron correlation near the Mott transition results in the lowness of ω_p^* at low temperatures and consequently promotes the Fröhlich interaction to form the polaronic Dirac electron state.

The enhancement of the polaronic state is often seen in correlated electron oxides near the Mott transition. In general, the electron correlation somewhat promotes the short-range electron-phonon interaction and formation of the small polaron [34]. Although the present results appear to be different from the conventional case, we cannot exclude the possibility of a mixture of the small polaron character from the above results alone. A remarkable feature of the small polaron is the effect of quenched disorder; the disorder promotes the self-trapping of the small polaron [35], which could be observed as the change in the polaron band.

To address this issue, we explored the doping variation of the polaron band for $CaIr_{1-x}Rh_xO_3$, wherein the doped Rh mainly acts as the quenched disorder. As shown in Fig. 4(a), the resistivity of the doped system shows a similar temperature dependence with that of $x = 0$, but the electron mobility significantly decreases with increasing x [see the inset to Fig. 4(a)], suggesting the enhancement of electron scattering. Figures 4(b)–4(d) show the $\sigma(\omega)$ spectra measured at 50 K. Both the Drude response and the polaron band are observed even in the doped system. As shown in Fig. 4(e), the spectral weight of the polaron band decreases with increasing x, but the Drude weight increases in accord with the modest enhancement of carrier density [19], leading to the reduction of $1 + \lambda$. The result can be straightforwardly understood by the Fröhlich polaron model and the signature of self-trapping of the small polaron is not discernible. A possible reason may be that electrons with a tiny Fermi surface in the present system is less amenable to the deformation potential due to the acoustic phonons with large momentum, which is a typical source of short-range electron-phonon interaction [36].

In summary, we have explored the charge dynamics of the correlated Dirac semimetallic $CaIrO_3$ by means of optical spectroscopy. The optical conductivity exhibits the ω-linear-type interband transition and the Drude weight monotonically decreases with lowering temperatures, which is consistent with the experimentally observed fact that the Fermi energy is nearly pinned to the line node due to the strong electron correlation near the Mott transition. We found that the absorption band of the large polaron with intermediate coupling strength appears at around 0.04 eV in the low temperature regime, where the plasma frequency is lower than the energy of relevant longitudinal phonons. These results suggest that the correlated Dirac electron forms the large polaron near the Mott criticality as the Fröhlich-type electron-phonon interaction becomes appreciable via the insufficient screening of optical phonons due to the dilute carrier density and reduced Fermi velocity. Although the electron-phonon interaction is not likely strong enough to change the topology of the line node at the present state, it could be a unique knob to induce other topological phases, when the Dirac electron is quasi-one-dimensionally confined in the quantum limit.

We thank M. Kawamura, S. Sakai, M. Hirayama, R. Arita, M. Hoshino, and D. Hashizume for useful discussions. This work was partly supported by Grant-In-Aid for Science Research (Grants No. 16H00981, No. 18H01171, No. 18H04214, and No. 16H06345) from the MEXT, and by PRESTO (Grant No. JPMJPR15R5) and CREST (Grant No. JPMJCR16F1), JST, Japan.

[1] N. P. Armitage, E. J. Mele, and A. Vishwanath, Rev. Mod. Phys. **90**, 015001 (2018).
[2] H. Wei, S-P. Chao and V. Aji, Phys. Rev. Lett. **109**, 196403(R) (2012).
[3] Z. Wang and S. C. Zhang, Phys. Rev. B **87**, 161107(R) (2013).
[4] B. Roy and J. D. Sau, Phys. Rev. B **92**, 125141 (2015).
[5] Z. Song, Z. Fang, and X. Dai, Phys. Rev. B **96**, 235104 (2017).
[6] J. Gooth *et al.*, Nature (London) **575**, 315 (2019).
[7] X. Wan, A. M. Turner, A. Vishwanath, and S. Y. Savrasov, Phys. Rev. B **83**, 205101 (2011).
[8] W. Witczak-Krempa and Y. B. Kim, Phys. Rev. B **85**, 045124 (2012).
[9] R. Schaffer, E. Kin-Ho Lee, B.-J. Yang, and Y. B. Kim, Rep. Prog. Phys. **79**, 094504 (2016).
[10] J.-M. Carter, V. V. Shankar, M. A. Zeb, and H.-Y. Kee, Phys. Rev. B **85**, 115105 (2012).

[11] C. L. McDaniel and S. J. Schneider, J. Solid State Chem. **4**, 275 (1972).
[12] J. M. Longo, J. A. Kafalas, and R. J. Arnott, J. Solid State Chem. **3**, 174 (1971).
[13] J.-G. Cheng, T. Ishii, H. Kojitani, K. Matsubayashi, A. Matsuo, X. Li, Y. Shirako, J.-S. Zhou, J. B. Goodenough, C. Q. Jin, M. Akaogi, and Y. Uwatoko, Phys. Rev. B **88**, 205114 (2013).
[14] H. Zhang, K. Haule, and D. VanderbiltPhys. Rev. Lett. **111**, 246402 (2013).
[15] M. Imada, A. Fujimori, and Y. Tokura, Rev. Mod. Phys. **70**, 1039 (1998).
[16] J. Fujioka, R. Yamada, M. Kawamura, S. Sakai, M. Hirayama, R. Arita, T. Okawa, D. Hashizume, M. Hoshino, and Y. Tokura, Nat. Commun. **10**, 362 (2019).
[17] M. Masuko, J. Fujioka, M. Nakamura, M. Kawasaki, and Y. Tokura, APL Mater. **7**, 081115 (2019).
[18] R. Yamada, J. Fujioka, M. Kawamura, S. Sakai, M. Hirayama, R. Arita, T. Okawa, D. Hashizume, M. Hoshino, and Y. Tokura, Phys. Rev. Lett. **123**, 216601 (2019).
[19] See Supplemental Material at http://link.aps.org/supplemental/10.1103/PhysRevB.103.L041109 for additional information on reflectivity measurements, calculation of spectral intensity, and fitting analysis.
[20] S. J. Moon, H. Jin, K. W. Kim, W. S. Choi, Y. S. Lee, J. Yu, G. Cao, A. Sumi, H. Funakubo, C. Bernhard, and T. W. Noh, Phys. Rev. Lett. **101**, 226402 (2008).
[21] B. Xu *et al.*, Phys. Rev. B **93**, 121110(R) (2016).
[22] A. Akrap, M. Hakl, S. Tchoumakov, I. Crassee, J. Kuba, M.O. Goerbig, C.C. Homes, O. Caha, J. Novk, and F. Teppe, Phys. Rev. Lett. **117**, 136401 (2016).
[23] S. P. Mukherjee and J. P. Carbotte, Phys. Rev. B **95**, 214203 (2017).
[24] P. Hosur, S. A. Parameswaran, and A. Vishwanath, Phys. Rev. Lett. **108**, 046602 (2012).
[25] R. E. Throckmorton, J. Hofmann, E. Barnes, and S. Das Sarma, Phys. Rev. B **92**, 115101 (2015).
[26] C. J. Tabert, J. P. Carbotte, and E. J. Nicol, Phys. Rev. B **93**, 085426 (2016).
[27] S. I. Kimura, H. Yokoyama, H. Watanabe, J. Sichelschmidt, V. Suss, M. Schmidt, and C. Felser, Phys. Rev. B **96**, 075119 (2017).
[28] D. Neubauer, J. P. Carbotte, A. A. Nateprov, A. Lohle, M. Dressel, and A. V. Pronin, Phys. Rev. B **93**, 121202(R) (2016).
[29] N. M. R. Peres, R. M. Ribeiro, and A. H. Castro Neto, Phys. Rev. Lett. **105**, 055501 (2010).
[30] J. T. Devreese and A. S. Alexandrov, Rep. Prog. Phys. **72**, 066501 (2009).
[31] A. S. Mishchenko, N. Nagaosa, N. V. Prokofev, A. Sakamoto, and B. V. Svistunov, Phys. Rev. Lett. **91**, 236401 (2003).
[32] C. Verdi, F. Caruso, and F. Giustino, Nat. Commun. **8**, 15769 (2017).
[33] A. S. Mishchenko, N. V. Prokofev, A. Sakamoto, and B. V. Svistunov, Phys. Rev. B **62**, 6317 (2000).
[34] E. Dagotto, T. Hotta, and A. Moreo, Phys. Rep. **344**, 1 (2001).
[35] Y. Shinozuka and Y. Toyozawa, J. Phys. Soc. Jpn. **46**, 505 (1979).
[36] F. M. Peeters and J. T. Devreese, Phys. Rev. B **32**, 3515 (1985).